Synthesis, structural, electrical and thermal properties of Ti-doped $Bi_2Sn_2O_7$ pyrochlore

M. Roy · Indu Bala · S. K. Barbar

Abstract Polycrystalline ceramic samples of $Bi_2Sn_{2-x}Ti_xO_7$ ($x = 0.0, 0.2, 0.4, 0.6, 0.8$) have been synthesized by conventional solid-state reaction method. The effect of homovalent cation (titanium) substitution on the Sn-site on the structural, morphological, electrical and thermal properties of the pure $Bi_2Sn_2O_7$ ceramics have been studied by X-ray diffraction (XRD) followed by scanning electron microscopic techniques, dc conductivity and modulated differential scanning calorimetry. The XRD analysis carried out by performing the Rietveld refinement using the space group Fd3m indicates that the increase of titanium contents do not lead to any secondary phase. The grain size distributions of all the samples were investigated by SEM. It was found that the grain sizes are strongly influenced by the addition of titanium to the system. The frequency and temperature dependent dielectric studies have been carried out. The dc conductivity measurement was carried out for all the compounds and the activation energies were calculated using the relation $\sigma = \sigma 0 \exp(-E_a/kT)$. The modulated differential scanning calorimetry has been used to investigate the effect of substitution on the specific heat, heat flow and other thermal parameters of the compounds. The results are discussed in detail.

Keywords Ceramics · Sintering · X-ray diffraction · Dielectric properties · SEM · Electrical resistivity · DSC

M. Roy (✉) · I. Bala · S. K. Barbar
Department of Physics, M. L. Sukhadia University,
Udaipur 313002, Rajasthan, India
e-mail: mroy1959@yahoo.co.in

Introduction

The compound $Bi_2Sn_2O_7$ belongs to the pyrochlore family of general formula $A_2B_2O_7$ where A-cations are eight coordinated and B-cations are six coordinated. This structure of the mineral pyrochlore is adopted by a large number of mixed oxides such as $Bi_2Sn_2O_7$. Typically, A and B are metal ions in oxidation states III and IV or II and V, respectively. However, there are numerous other possibilities for the charge balance to be achieved, resulting in higher stoichiometric mixed oxides, as well as vacancy containing defect pyrochlores. From the standpoint of structural chemistry, the stability field of pyrochlore phases can be related to the rA:rB radius ratio. In general, the pyrochlore phase is stable up to rA:rB = 1.8; beyond this value the fluorite structure becomes more favourable. A detailed account of the structural stability field of pyrochlores, as well as chemical compositions that satisfy these requirements, is given in a review by Subramanian et al. [1]. In spite of the immense flexibility of chemical composition in the pyrochlore system, a cubic structure with eight molecules per unit cell ($Z = 8$) and space group Fd3m is the predominant phase. The compounds with pyrochlore structure having noncubic symmetry occur frequently in the case when A-cations are those with inert lone pairs of electrons, such as Bi, Pb and so on [2–4]. The series of rare-earth pyrochlore are of considerable importance for numerous applications including piezoelectricity, dielectric, resistance to radiation damage, and have been specially investigated as heterogeneous catalysts for a variety of processes. Pyrochlore-type bismuth tin oxide ($Bi_2Sn_2O_7$) was first reported by Roth [5]. It is a material with well established and important catalytic and gas-sensing properties such as a selective sensor for carbon monoxide in the presence of other gases [6–9]. It is the key

component of multiphasic catalysts for partial oxidation of isobutene to methacrolein [10–12]. In an early structural study by Brisse and Knop [13] $Bi_2Sn_2O_7$ was described as pyrochlore-related, with the diffraction pattern containing extra reflections that precluded cubic indexing. Owing to the diversity of their chemistry, pyrochlores display an array of interesting properties including ferroelectricity, oxide ion conduction, colossal magnetoresistance, spin ice behaviour, metal-to-insulator transitions, catalytic and gas-sensing properties [14–21]. In view of this, the present paper reports on the synthesis of highly resistive poly-crystalline ceramic samples of Pure and Ti-doped $Bi_2Sn_2O_7$ by optimizing the synthesis condition such as time, temperature etc. and its detailed structural, electrical and thermal properties.

Experimental

The polycrystalline ceramic samples of $Bi_2Sn_{2-x}Ti_xO_7$ ($x = 0.0$, 0.2, 0.4, 0.6 and 0.8) were prepared by high temperature solid-state reaction method under controlled time and temperature conditions. The stoichiometric mixture of Bi_2O_3, SnO_2 and TiO_2 (99.99 % pure obtained from HIMEDIA and CDH, Mumbai) were mixed thoroughly in a liquid medium for several hours and then calcined at 800–900 °C for 8 h in silica crucible under air atmosphere. In this study, an excess of (~ 2 wt%) bismuth oxide was added to the solution to minimize the bismuth loss during the thermal treatment at high temperature. The process of firing and grinding was repeated for a number of times. The resulting mixture was compressed into pellet form by applying pressure around 498 MPa using a hydraulic press. These pellets were sintered at 1,050 °C for 2 h. The sintered pellets were coated with silver paint to act as electrodes for the electrical measurements. Structural characterizations of the sintered powders were carried out by the X-ray diffraction method using Rigaku X-ray diffractometer with CuKα radiation and nickel filter in a wide range of 2θ from 10 to 90° with a scanning rate of 2° per minute. The instrument was calibrated using the pure silicon sample provided with the instrument. The lattice parameters and other structural information were obtained by the Rietveld refinement Fullprof program using a pseudo-voigt function [22]. The surface morphology and grain size of samples were measured by scanning electron microscopy using the JEOL, JSM-5600 SEM with different magnifications in back scattered mode. The dielectric constant (ε') was measured as a function of frequency (50 Hz–1 MHz) and temperature (300–673 K) in air atmosphere using a HIOKI 3532-50 LCR METER. The dc electrical conductivity measurement was carried out in the temperature range from RT to 673 K using the laboratory

made set up by two probe method. The MDSC measurement was carried out with a TA instruments Model 2910 from 400 to 840 K in inert (N_2) atmosphere with a heating rate of 5 K/min and ± 0.75 K modulation per 60 s.

Results and discussion

Figure 1 shows the XRD patterns of $Bi_2Sn_{2-x}Ti_xO_7$ ($x = 0.0$, 0.2, 0.4, 0.6, 0.8). The observed diffraction pattern for $x = 0.0$ is well matching with that of the standard data (Card No. JCPDS #17-0457) except two minor low-intensity impurity peaks at $2\theta = 24.61$ and 32.52°, which are due to the unreacted SnO_2 oxide and are corresponding to the JCPDS card numbers #02-1340 and #72-2324. All other XRD patterns are also showing these impurity peaks at same 2θ position. All these impurity peaks in XRD pattern are coming within the error limit of 2–5 %, which are not affecting the structural and physical properties of the compounds. The peaks in diffraction patterns were indexed in cubic structure having eight formula unit per unit cell ($z = 8$) with space group Fd3m. The Rietveld refinement analysis of all the patterns confirmed a cubic structure. From the X-ray diagram, it is also observed that there is no change in peak positions for the substituted compounds. This shows that the $Bi_2Sn_{2-x}Ti_xO_7$ system exhibits solid solution behaviour and all the pure and substituted compounds have the same crystal symmetry. Therefore, all these samples show the similar basic XRD pattern.

The lattice parameters and other structural parameters are tabulated in Table 1. The detailed Rietveld refinement of all the compounds is described elsewhere [23]. The interplaner spacings (d-values) have been calculated based
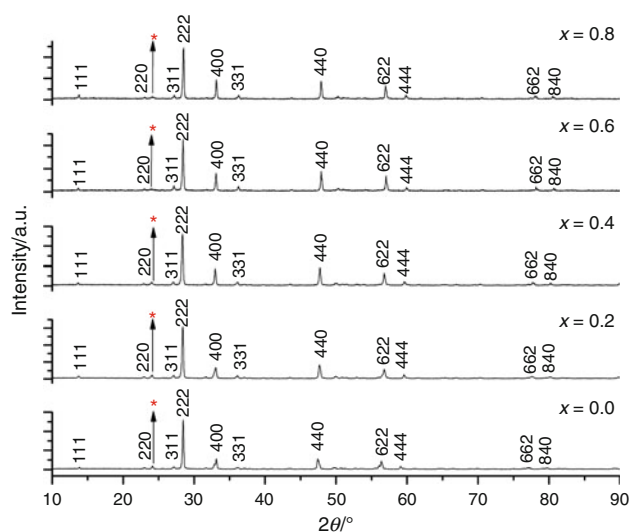

Fig. 1 RT X-ray diffraction patterns of $Bi_2Sn_{2-x}Ti_xO_7$ ($x = 0.0$, 0.2, 0.4, 0.6 and 0.8)

Table 1 Structural and electrical parameters of Bi$_2$Sn$_{2-x}$Ti$_x$O7 (x = 0.0, 0.2, 0.4, 0.6 and 0.8)

Concentration/x	Grain size/μm	$a = b = c$/Å	Density/ g cm^{-3}	E_a/eV
0.0	2-5	10.6583	4.917	1.38
0.2	2-3	10.6308	5.732	1.07
0.4	2-3	10.6259	7.449	1.03
0.6	1-2	10.5897	7.490	1.02
0.8	1-2	10.5575	7.889	0.79

on the refined cell parameters and these calculated d-values are well matching with the observed d-values. When Sn-site is substituted with homovalent cation Ti^{4+} (x = 0.2), the diffraction patterns are quite similar with the same impurity peaks as shown in Fig. 1. The only difference observed in all the diffraction patterns is that the solder (doublet) in 400 and 622 peaks observed in the case of pure compound (x = 0.0) have become a single intense peak with the increase of substitution concentration up to x = 0.8. This is the experimental signature of the presence of Ti^{4+} on the Sn^{4+} site. Further it is observed that with the increase of Ti^{4+} concentration on the Sn-site, the lattice parameters as well as the interplanar spacings (d-values) decrease (Table 2). This decrease in d-spacings and lattice parameters may be explained on the basis of difference in ionic radius of Ti^{4+} and Sn$^{4+.}$ As the ionic radius of Ti^{4+} (0.605 Å) is smaller than that of the Sn^{4+} (0.69 Å) and hence with the increase of Ti^{4+} ion on the Sn-site the d-spacings (Table 2) as well as the lattice parameters are decreasing. The density was measured by the usual volume and weight measurement technique. The density of Ti-doped samples is slightly higher than the pure Bi$_2$Sn$_2$O$_7$ (Table 1). The morphological and microstructural analysis revealed that the distributions of grains are almost uniform except few grains which are of larger size throughout the surface for all the samples. The incorporation of Ti^{4+} ions on the Sn^{4+} site into the crystal lattice of Bi$_2$Sn$_2$O$_7$ is responsible for suppression of vacancy formation due to bismuth loss and grain growth reduced. As Ti^{4+} concentration increased, preferred orientation of the grain reduced and this reduction in the preferred grain orientation seems to be associated with the decrease in grain size. Hence, a continuous decrease in the grain size with the increase of Ti^{4+} ions has been observed and are shown in Table 1. The typical SEM micrographs of all the samples are shown in Fig. 2a–e.

The variation of dielectric constant with frequency at room temperature (Fig. 3) indicates that the dielectric constant decreases rapidly at lower frequencies while it remains almost constant at higher frequencies. It is believed that defects such as oxygen vacancies inherently present in these materials due to the volatilization of Bi–O species create space charges whose polarization can respond to the external electric field. At low frequencies, these charges have enough time to move longer distances in the sample, creating a larger electronic polarization. Therefore, a high value of (apparent) dielectric constant is measured. At higher frequencies the space charges no longer follow the field leading to lower values of dielectric constant. This variation of dielectric constant at lower frequencies is attributed not due to the electronic and ionic contribution but due to the space charge contribution. While with the increase of frequency the ionic and electronic contribution becomes dominant and space charge contribution diminishes gradually and hence dielectric constant decreases with increase of frequency and attains almost constant value at higher frequencies.

The variation of the dielectric constant (ε') with the temperature at a frequency of 100 kHz is shown in Fig. 4. The

Table 2 Comparison between some of the observed and calculated d-values (Å) for Bi$_2$Sn$_{2-x}$Ti$_x$O7 (x = 0.0, 0.2, 0.4, 0.6 and 0.8)

x = 0.0		x = 0.2		x = 0.4		x = 0.6		x = 0.8		hkl
d-obs/Å	d-cal/Å	d-obs/Å	d-cal/Å	d-obs/Å	d-cal/Å	d-obs/Å	d-cal/Å	d-obs/Å	d-cal/Å	
6.156	6.153	6.140	6.137	6.137	6.135	6.116	6.114	6.098	6.095	111
3.769	3.768	3.760	3.758	3.758	3.756	3.745	3.744	3.734	3.732	220
3.214	3.213	3.206	3.205	3.205	3.204	3.194	3.193	3.184	3.183	311
3.078	3.076	3.070	3.069	3.068	3.067	3.058	3.057	3.049	3.047	222
2.665	2.664	2.658	2.657	2.657	2.656	2.648	2.647	2.640	2.639	400
2.446	2.445	2.439	2.439	2.438	2.437	2.430	2.429	2.423	2.422	331
1.884	1.884	1.880	1.879	1.879	1.878	1.872	1.872	1.867	1.866	440
1.607	1.606	1.603	1.603	1.602	1.602	1.597	1.596	1.592	1.591	622
1.538	1.538	1.535	1.534	1.534	1.534	1.529	1.528	1.524	1.523	444
1.223	1.222	1.219	1.219	1.219	1.218	1.215	1.214	1.211	1.211	662
1.192	1.191	1.188	1.188	1.188	1.188	1.184	1.184	1.180	1.180	840

Fig. 2 a–e SEM micrographs of $Bi_2Sn_{2-x}Ti_xO_7$ ($x = 0.0$, 0.2, 0.4, 0.6, 0.8)
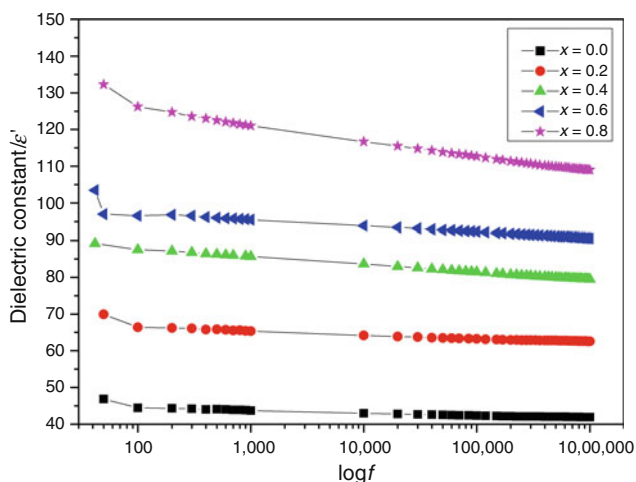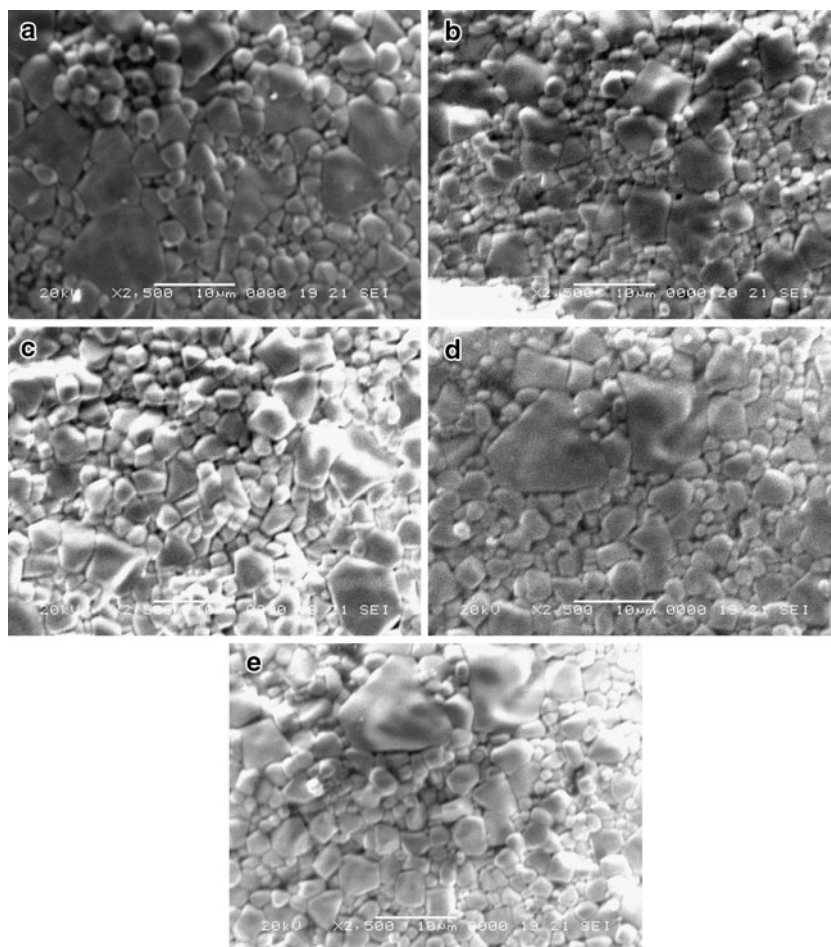
Fig. 3 Dielectric constant versus frequency curves of $Bi_2Sn_{2-x}Ti_xO_7$ ($x = 0.0$, 0.2, 0.4, 0.6 and 0.8)

Fig. 4 Dielectric constant versus temperature curves of $Bi_2Sn_{2-x-}Ti_xO_7$ ($x = 0.0$, 0.2, 0.4, 0.6, 0.8)

dielectric constant shows an increasing trend with the increase of temperature but no phase transition has been observed up to the measured temperature range in all the compounds of $Bi_2Sn_{2-x}Ti_xO_7$. Ti-doping increases the dielectric constant and hence improving the electrical insulation characteristics.

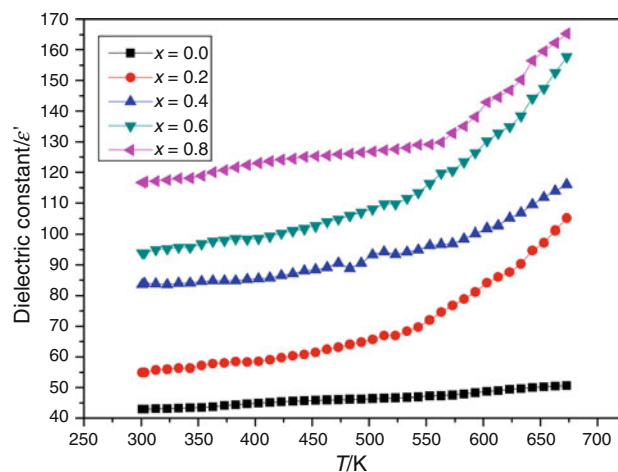With increasing temperature the effect of charge polarization is enhanced, giving rise to higher (apparent) permittivity values. As the temperature is further increased, more dipoles in the sample are able to switch leading to an increase in the apparent dielectric constant.

The temperature dependence of dc electrical conductivity (σ_{dc}) for $Bi_2Sn_{2-x}Ti-O_7$ ($x = 0.0, 0.2, 0.4, 0.6$ and 0.8) has been evaluated by taking the steady-state values of current and results are plotted for temperature ranging from
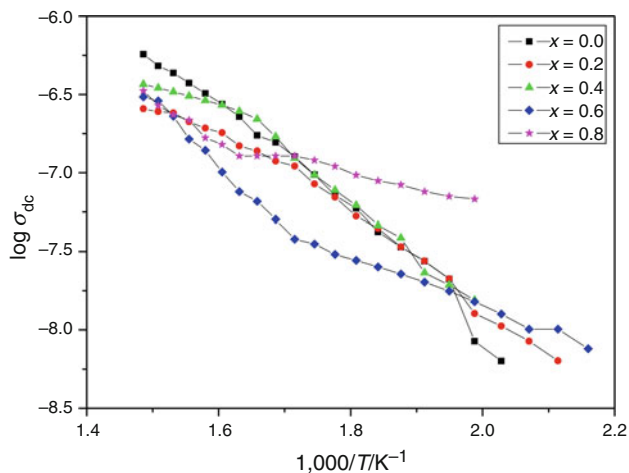
480 to 673 K as shown in Fig. 5. The conductivity is almost constant below 480 K in almost all cases hence the results are plotted for an elevated temperature range from 480 to 673 K. This shows that the quality of our samples is better and more resistive. It is well-known that the electrical conduction in solids may be explained using the energy band model employing the appropriate scattering mechanism. In a narrow band solid the electron–electron correlation and electron–phonon coupling becomes important and the charge carriers are localized responsible for the conduction arising through hopping mechanism. The conduction due to impurities, defects etc. takes place either through band mechanism or through hopping of the charge carriers among impurity centres. In the present case, the increase in conductivity may be explained by the fact that it is a consequence of thermally activated process which can be described by the Arrhenius relation: $\sigma = \sigma_0 \exp(-E_a/kT)$, where σ_0 is the pre-exponential factor, E_a is the activation energy and k is the Boltzmann constant having the value $k = 8.65 \times 10^{-5}$ eV K^{-1}. By observing the log σ_{dc} versus $1,000/T$ plot and the calculated activation energy (Table 1) of all the pure and substituted

Fig. 5 log σ_{dc} versus $1,000/T$ curves of $Bi_2Sn_{2-x}Ti_xO_7$ ($x = 0.0, 0.2, 0.4, 0.6$ and 0.8)

Fig. 6 a–e Heat capacity and heat flow versus temperature curves of $Bi_2Sn_{2-x}Ti_xO_7$ ($x = 0.0, 0.2, 0.4, 0.6$ and 0.8)
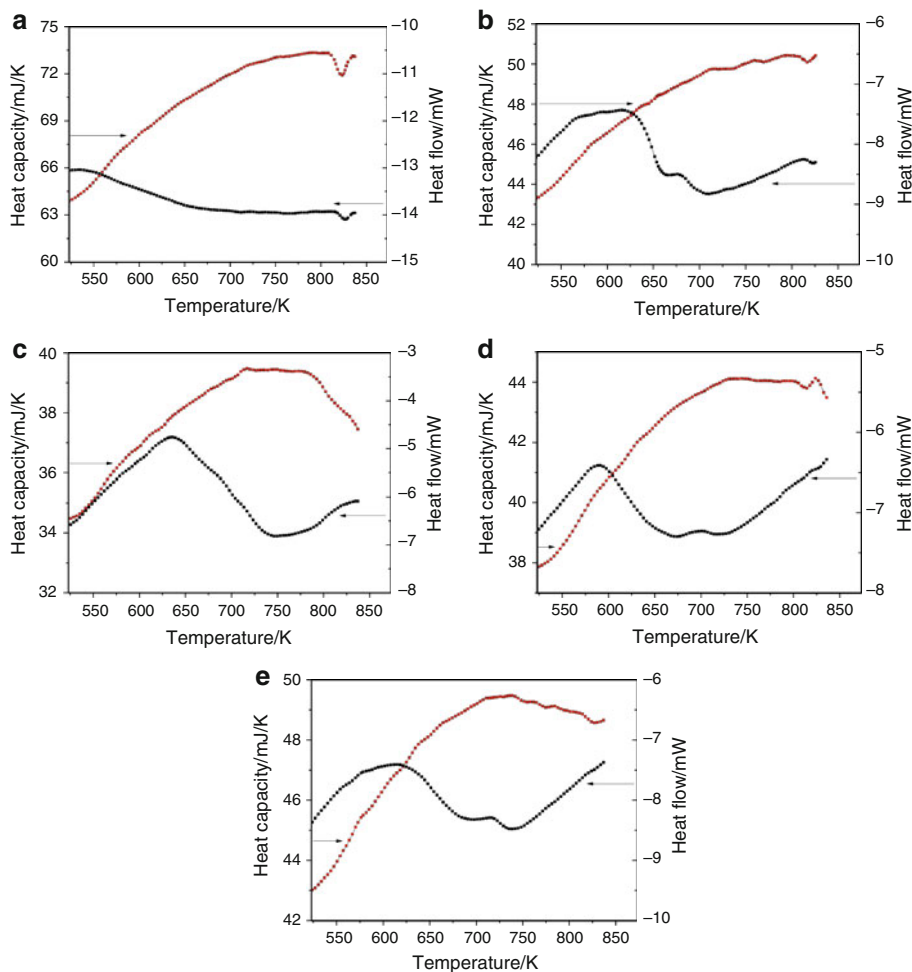
compounds, it seems that from *RT* to around 480 K all the compounds show relaxation behaviour which may be explained due to polarization of charge carriers and beyond that activation energy decreases with the increase of Ti^{4+} content up to $x = 0.8$. The increase in resistivity for $x = 0.6$ and $x = 0.8$ may be explained on the basis of bond stability of Ti–O and Sn–O bonds. Since Ti–O bond is more stable than Sn–O bond and hence log σ_{dc} versus $1/T$ curve shows decrease in conductivity as well as relaxation behaviour with the increase of Ti content in place of Sn.

Figure 6a–e shows MDSC curves of $Bi_2Sn_{2-x}Ti_xO_7$ ($x = 0.0$, 0.2, 0.4, 0.6 and 0.8) where heat capacity and heat flow have been measured as a function of temperature (523–843 K). For pure compound ($x = 0.0$), the MDSC curve shows a sharp endothermic peak both in heat capacity and heat flow curve around 825 K. This endothermic peak around 825 K may be due to structural phase transition from ordered γ phase to the more disordered γ' phase of the compound. For $x = 0.2$, the heat capacity curve indicates an exothermic peak at 713 K while the heat flow curve indicates endothermic peak around 710 K. The compound also shows an endothermic peak at 816 k in heat capacity curve and an exothermic peak around 814 K in heat flow curve. The compound of concentration $x = 0.4$ shows a broad exothermic peak around 634 K as well as a broad endothermic peak at 747 K while the heat capacity curve shows a very small exothermic peak around 713 K with a broad hump around 775 K. For $x = 0.6$, the heat flow curve shows a broad exothermic peak at 590 K followed by a shallow peak (exothermic) around 700 K. The curve also shows a small kink (endo-) around 823 K. The heat capacity curve shows a broad hump (exo-) around 733 k followed by a sharp exothermic peak at 823 K. Further increase of Ti concentration from $x = 0.6$ to $x = 0.8$, the MDSC curve shows a small exothermic peak in heat capacity curve and broad endothermic peak in heat flow curve at temperature around 745 K. Not only this, the heat capacity curve shows an endothermic peak at 825 K which is absent in heat flow curve. The peaks observed below 825 K for $x = 0.4$, 0.6 and 0.8 are still to be identified by some other thermal techniques. The detailed analysis of all the identified peaks in heat flow and heat capacity curves in all the Ti^{4+} substituted compounds need further explanation and are in progress which will be published as pert II of this paper concentrated fully on detailed thermal analysis.

Conclusions

From the above studies it is concluded that with the increase of Ti^{4+} concentration on the Sn^{4+} site, the lattice parameters as well as the interplanar spacings (*d*-values)

decreases. It is also concluded that the grain size decreases with the increase of Ti^{4+} ion on the Sn^{4+} site which is also responsible for the enhanced dielectic constant of the substituted materials. It is found that the conductivity of the system is strongly influenced by titanium addition. The thermal parameter such as heat capacity and heat flow of all the materials were examined as a function of temperature.

References

1. Subramanian MA, Aravamudan G, Subba Rao GV. Oxide pyrochlores—a review. Prog Solid State Chem. 1983;15:55–143.
2. Vetter G, Queyroux F, Gilles JC. Preparation, stabilite et etude cristallographique preliminaire du compose Bi₂Sn₂O₇. Mater Res Bull. 1978;13:211–6.
3. Shannon RD, Bierlein JD, Gillson JL, Jones GA, Sleight AW. Polymorphism in Bi₂Sn₂O₇. J Phys Chem Solids. 1980;41:117–22.
4. Sulcova P, Vecera J, Bystrzycki P. Thermal analysis of doped Bi₂O₃. J Therm Anal Calorim. 2012;108:525–9.
5. Roth RS. Pyrochlore-type compounds containing double oxides of trivalent and tetravalent ions. J Res Natl Bur Stand. 1956;56:17–25.
6. Moens L, Ruiz P, Delmon B, Devillers M. Enhancement of total oxidation of isobutene on bismuth-promoted tin oxide catalysts. Catal Lett. 1997;46:93–9.
7. Mones L, Ruiz P, Delmon B, Devillers M. Cooperation effects towards partial oxidation of isobutene in multiphasic catalysts based on bismuth pyrostannate. Appl Catal A. 1998;171:131–43.
8. Mones L, Ruiz P, Delmon B, Devillers M. Enhancement of total oxidation of isobutene on bismuth-promoted tin oxide catalysts. Appl Catal A. 1999;180:299–315.
9. Coles GSV, Bond SE, Williams G. Metal stannates and their role as potential gas-sensing elements. J Mater Chem. 1994;4:23–7.
10. Devi GS, Manorama SV, Rao VJ. SnO₂/Bi₂O₃: a suitable system for selective carbon monoxide detection. J Electrochem Soc. 1998;145:1039–44.
11. Devi GS, Manorama SV, Rao VJ. SnO₂:Bi₂O₃ based CO sensor: laser-Raman, temperature programmed desorption and X-ray photoelectron spectroscopic studies. Sens Actuators B. 1999;56:98–105.
12. Malinovskaya TD, Aparnev AI, Egorov YP, Yukhin YM. Carbon monoxide semiconductor sensors based on SnO₂–Bi₂O₃. Russ J Appl Chem. 2001;11:1864–7.
13. Brisse F, Knop O. Pyrochlores. III. X-ray, neutron, infrared and dielectric studies of A₂Ti₂O₇ titanates. Can J Chem. 1968;46:859–73.
14. Cook WR, Jaffe H. Ferroelectricity in oxides of fluorite structure. Phys Rev. 1952;88:1426.
15. Van Dijk MP, de Vries KJ, Burggraaf AJ. Oxygen ion and mixed conductivity in compounds with the fluorite and pyrochlore structure. Solid State Ion. 1983;9–10:913–9.
16. Bernik S, Daneu N. Characteristics of SnO₂-doped ZnO based varistor ceramics. J Eur Ceram Soc. 2001;21:1879–82.

17. Mergen A, Zorlu H, Özdemir M, Yumak M. Fabrication and characterisation of Cr and Co-doped $Bi_{1.5}Zn_{0.92}Nb_{1.5}O_{6.92}$ pyrochlores. J Eur Ceram Soc. 2011;31:2633–9.

18. Chen Y-C, Cheng H-F, Tsau Y-M, Kužel P, Petzelt J, Lin I-N. Synthesis and properties of dielectric $Bi_2(Zn_{1/3}Nb_{2/3})_2O_7$ thin films. J Eur Ceram Soc. 2001;21:2731–4.

19. West AR. Solid state chemistry and its applications. New Delhi: Wiley; 1988.

20. Kan A, Ogawa H, Inami Y, Moriyama T. Synthesis and ferroelectric properties of bismuth layer-structured $(Bi_{7-x}Sr_x)(Fe_{3-x}Ti_{3+x})O_{21}$ solid solutions. Phys B. 2011;406:3170–4.

21. Abdelkhalek SB, Kallel N, Kallel S, Guizouarn T, Peña O, Oumezzine M. Transport behavior and mechanism of conduction of simultaneously substituted Y and Fe in $La_{0.7}Ba_{0.3}MnO_3$ perovskite. Phys B. 2011;406:4060–7.

22. Rodriguez-Carvajal J. Recent developments of the program Fullprof, in commission on powder diffraction. IUCr Newslett. 2001;26:12–9.

23. InduBala, Barbar S.K., Roy M., Synthesis, structural and electrical properties of Ti modified $Bi_2Sn_2O_7$ pyrochlore. Phys B. 2012. doi:10.1016/jphysb.2012.05.011.